Applied Physics Letters ARTICLE scitation.org/journal/apl

Existence and stability of skyrmion bags in thin magnetic films

Cite as: Appl. Phys. Lett. **116**, 022413 (2020); doi: 10.1063/1.5127173
Submitted: 15 September 2019 · Accepted: 16 December 2019 ·
Published Online: 16 January 2020

Charles Kind,[1,a)] Sven Friedemann,[2] and Dan Read[3]

AFFILIATIONS

[1]School of Mathematics, University of Bristol, Bristol BS8 1TW, United Kingdom
[2]HH Wills Physics Laboratory, University of Bristol, Bristol BS8 1TL, United Kingdom
[3]School of Physics and Astronomy, Cardiff University, Cardiff CF24 3AA, United Kingdom

[a)]charles.kind@bristol.ac.uk

ABSTRACT

Skyrmion bags are spin textures of any integer topological degree, realized in micromagnetic simulations and experimentally in liquid crystals. They have been proposed as a promising new form of magnetic data storage due to their stability with respect to perturbations and the possibility of encoding different values in topologically distinct magnetization configurations. We simulate skyrmion bags in magnetic thin films having a range of physically realistic material parameters. The results give a range over which stable skyrmion bags may be found in experiment, and we extract a relationship to help guide the production of these potentially useful quasiparticles.

Individual magnetic skyrmions are stable, particle-like, spin configurations in the magnetization of chiral magnets.[1] Their stability is derived from the skyrmion's topological nature. A single skyrmion in the continuous model is a perfect cover of the two-sphere, illustrated in Fig. 1(c), and hence impossible to unwind. This stability, coupled with the low currents required to move them, makes them seem to be attractive as candidates for future forms of magnetic data storage with read-write capabilities.[2]

Skyrmions have been observed with radii on the order of nanometers, and due to the relative weakness of inter-skyrmion reactions, they can be densely packed. A single skyrmion can, however, only represent a binary bit, in current racetrack models,[3] where the change in the distance between skyrmions could lead to data loss. Hence, the interest in higher topological degree skyrmions which could encode more data per texture and yet retain the benefits of unitary degree skyrmions.[4,5]

Skyrmion bags,[4] or sacks,[5] are nested skyrmionic structures of any integer topological degree, typically composed of a single skyrmion outer boundary and then a number of inner antiskyrmions, which can themselves contain skyrmions. This pattern may continue with skyrmions or antiskyrmions contained within their opposing degree partners. In two dimensional (2D) models describing thin films, bags can be described by the total topological degree defined as

$$Q = \frac{1}{4\pi}\int \boldsymbol{n}\cdot\left(\partial_x\boldsymbol{n}\times\partial_y\boldsymbol{n}\right)dxdy, \tag{1}$$

where $\boldsymbol{n}(\boldsymbol{x})$ is the unit vector field of magnetization. With this definition, a single skyrmion has the degree $Q=-1$.

Skyrmion bags, being composed of any number of skyrmions and antiskyrmions, could give rise to an infinite variety of bag configurations at any degree. We use a notation to define the degree of each grouping of (anti)skyrmions within the bag. An $S(n)$ bag is the one with n antiskyrmions and a total degree of $Q=n-1$. As an antiskyrmion's degree has an opposite sign to a skyrmion, structures like the $S(1)$ bag, shown in **1d**, also known as skyrmionium or target skyrmions,[6,7] have a total degree of zero.

Skyrmions and, as we show here, skyrmion bags occur in magnetic materials with inversion asymmetry. In materials with uniaxial anisotropy, which we consider here, they can have either a Néel or Bloch type, shown in Figs. 1(a) and 1(b), respectively, determined by the dominant type of Dzyaloshinskii–Moriya interaction (DMI) present. In thin film multilayers, the DMI results in Néel type skyrmions, when projected onto the two spheres, have vectors normal to the surface and have been called hedgehog skyrmions.[8] In this paper, we look exclusively at Néel type skyrmions, but the technique illustrated here could also be applied in Bloch type configurations.

In thin films hosting skyrmions, the magnetic characteristics can be tuned through changes in the composition and thicknesses of individual layers. The magnetic properties of the ferromagnetic material sandwiched between heavy metal layers can be altered.[9] DMI interactions, which are caused by spin–orbit coupling (SOC), can be tuned.[10]

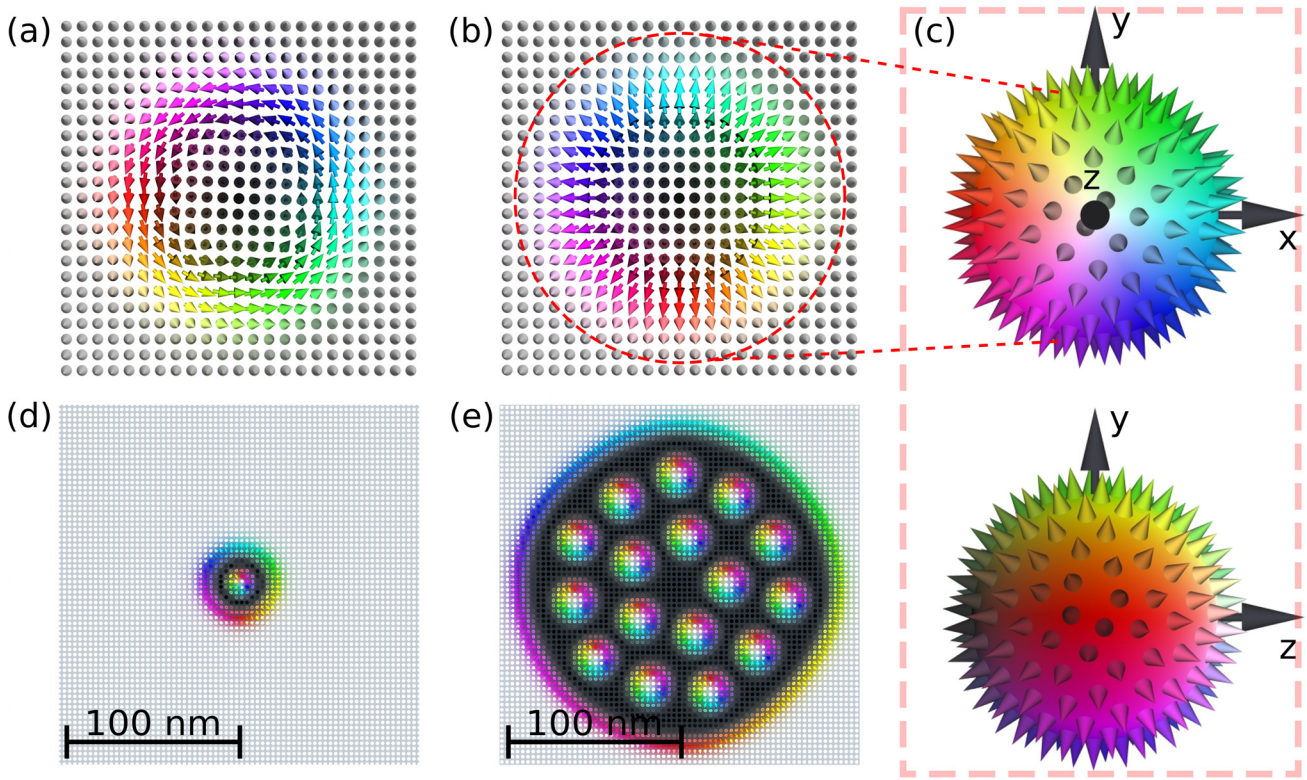

FIG. 1. Skyrmion and skyrmion bag configurations. (a) A Bloch skyrmion. (b) A Néel skyrmion. (c) The Runge color sphere with spins pointing normal to the surface. The top sphere representing the mapping of the Neèl skyrmion (b) to S^2, assuming that the marked path contains only unit vectors in the $+e_z$ direction. (d) A stable Mumax3 simulated $S(1)$ bag for constants $A_{ex} = 10$ pJ m^{-1}, $D_{\mathrm{DMI}} = 2.5$ mJ m^{-2}, and $K_u = 0.7$ MJ m^{-3} on a 1024×1024 nm^2 square of thickness 1 nm with a fixed boundary. (e) A stable Mumax3 simulated $S(16)$ bag for the same constants and domain as in (d).

The thickness of the magnetic layer can also affect DMI and the demagnetizing field. More subtle variation of the DMI in thin films produced via magnetron sputtering has also been reported by varying the thickness of an adjacent oxide layer[11] or by modifying the deposition conditions such as sputter chamber base pressure.[12] Magnetocrystalline anisotropy, which also derives from SOC, can also be altered in these multilayers.[13]

In this Letter, using micromagnetic simulations, we analyze skyrmion bags for a range of physical constants that are relevant to known experimentally realized magnetic multilayers such as CoPt, see Table I. With a range of permissible magnetic parameters, we show where we may find skyrmion bags.

TABLE I. Magnetic parameters for materials hosting skyrmions.

Exchange A_{ex} pJ m^{-1}	DMI D_{DMI} mJ m^{-2}	Anisotropy K_u MJ m^{-3}	Material	References
8	0.1	2	FePt	14
14	1.68	0.779	Pt/CoFeB/MgO	15
15	3	0.8	CoPt	14
20	4	0.8	CoFeB	16

The simulations were performed using the GPU-accelerated micromagnetic simulation program MuMax3[17] with Landau–Lifshitz dynamics in the form

$$\frac{\partial \boldsymbol{n}}{\partial t} = \gamma \frac{1}{1+\alpha^2}(\boldsymbol{n} \times \boldsymbol{B}_{\mathrm{eff}} + \alpha \boldsymbol{n} \times (\boldsymbol{n} \times \boldsymbol{B}_{\mathrm{eff}})), \tag{2}$$

where $\gamma \approx 176$ rad(ns T)$^{-1}$ is the electron gyromagnetic ratio, $\alpha = 0.3$ the dimensionless damping parameter, $\boldsymbol{B}_{\mathrm{eff}} = \delta E/\delta \boldsymbol{n}$ the effective magnetic field, and $\boldsymbol{n}(\boldsymbol{x}) = \boldsymbol{N}(\boldsymbol{x})/M_s$ the magnetization vector field normalized by saturation magnetization. The initial bag configurations were built from template functions of individual skyrmions and antiskyrmions, in the $S(1)$ and $S(16)$ configurations. The simulations showed a significant drop in energy from the initial condition, which indicates that the system achieves stability. These bags were chosen to represent experimentally realized skyrmionium, $S(1)$, and to explore the potential for skyrmion bags with a large range of data encoding, $S(16)$, which is expected to be more stable than $S(1)$.[4] Sixteen distinct configurations allow for the encoding of 4 bits of data.

The micromagnetic energy functional is evaluated as

$$E(\boldsymbol{n}) = E_{\mathrm{ex}} + E_{\mathrm{DMI}} + E_{\mathrm{demag}} + E_{\mathrm{anis}}, \tag{3}$$

where

$$E_{ex} = A_{ex} \int (\nabla \boldsymbol{n})^2 \, dxdy, \tag{4}$$

$$E_{DMI} = D_{DMI} \int [n_z(\nabla \cdot \boldsymbol{n}) - (\boldsymbol{n} \cdot \nabla) n_z] \, dxdy, \tag{5}$$

$$E_{demag} = \mu_0 M_s/2 \int (\boldsymbol{H}_{demag} \cdot \boldsymbol{n}) \, dxdy, \tag{6}$$

$$E_{anis} = K_u \int (1 - (n_z)^2) \, dxdy, \quad K_u > 0, \tag{7}$$

with these being the Heisenberg exchange, antisymmetric exchange (DMI), demagnetization, and easy axis anisotropy energies, respectively. $\boldsymbol{H}_{demag}$, in Eq. (6) is the demagnetizing field, which is calculated from the magnetization at each time step.[17]

The simulation geometry is a $1024 \times 1024\,nm^2$ square of thickness 1 nm, in order to represent a typical wire that could be fabricated using lithographic processing. A cell size of $2 \times 2 \times 1\ nm^3$ has been used. Uniform material parameters are a saturation magnetization of $M_s = 580\ kAm^{-1}$[14] and the uniaxial anisotropy is along the $+z$ direction, normal to the film. Exchange is selected from $\{10, 15, 20\}$ pJ m^{-1}, and interfacial DMI is in the range $[2, 4.3]$ mJ m^{-2} in steps of 0.1 mJ m^{-2} and uniaxial anisotropy $[0.6, 0.8]$ MJ m^{-3} in steps of 0.05 MJ m^{-3} to cover the range of possible material parameters (Table I).

The simulations used Mumax3's periodic boundary conditions and were run to simulate 100 ns with the vector field analyzed every one ns to test if the magnetization remains stable over time and to calculate the topological degree (1). At each grouping of constants, we test $S(1)$ and $S(16)$ bags [Figs. 1(d) and 1(e)] for stability. A structure was considered stable if the measured total energy varied by less than one part in 10^5 for at least 10 ns. Typically, stable structures would achieve equilibrium within 20 ns of the start of the simulation.

In order to guide our search for micromagnetic regimes where skyrmion bags could be stable, we seek a family of parameters A_{ex}, D_{DMI}, K_u that have comparable minimum energy magnetization configurations $\boldsymbol{n}(\boldsymbol{x})$. A Derrick scaling argument[18] on the energy functional (3) provides us with an expected stability condition. Perturbing the magnetization by rescaling space defining $\boldsymbol{n}_\lambda(x) = \boldsymbol{n}(\lambda x)$, where λ is an arbitrary constant, gives

$$E_\lambda = A_{ex} I_1 + D_{DMI} I_2/\lambda + K_u I_3/\lambda^2, \tag{8}$$

where

$$I_1 = \int (\nabla \boldsymbol{n})^2 dxdy, \tag{9}$$

$$I_2 = \int [n_z(\nabla \cdot \boldsymbol{n}) - (\boldsymbol{n} \cdot \nabla) n_z] dxdy, \tag{10}$$

$$I_3 = \int (1 - (n_z)^2) dxdy \text{ for } (x, y) \in \mathbb{R}^2. \tag{11}$$

If $(dE_\lambda/d\lambda)|_{\lambda=1} = -D_{DMI} I_2 - 2K_u I_3 = 0$, then stable skyrmions exist and

$$K_u = -D_{DMI} I_2/2I_3 = m \cdot D_{DMI}. \tag{12}$$

This is a type of virial constraint.[19] Therefore, we expect to find the same magnetization configurations at critical points of the energy functional as we follow the integral curve (12) varying the coefficients of anisotropy and DMI. We note that this equation is in the form of a straight line with slope m through the origin. In the Derrick scaling, we exclude the demagnetization term as is often done in micromagnetic energy functional analysis.[5] However, by analyzing the stability range obtained in our simulations with a straight line as shown in Eq. (12), we include the demagnetization as an effective anisotropy.[20,21] Indeed, we find good correspondence of our results to Eq. (12).

In Fig. 2, we show the range of K_u and D_{DMI} for $A_{ex} = 20$ pJ m^{-1}. Stable $S(1)$ and $S(16)$ bags are found roughly along a straight line through the origin as expected based upon our Derrick scaling analysis. We tabulate the slopes of the center lines of $S(1)$ and $S(16)$ bags for all simulated A_{ex} in Table II. We find the central gradient line for a bag type, $S(1)$ or $S(16)$, at a particular exchange energy, by finding the gradient at each data point, summing over all relevant points and dividing by the total number. We assume that the gradients are normally distributed, supported by Q-Q plots and Anderson Darling,[22] and record the results.

Our results indicate that the $|2\sigma|$ range of $S(1)$ is entirely encompassed by the $|2\sigma|$ range for the $S(16)$ bags, at all exchange constants

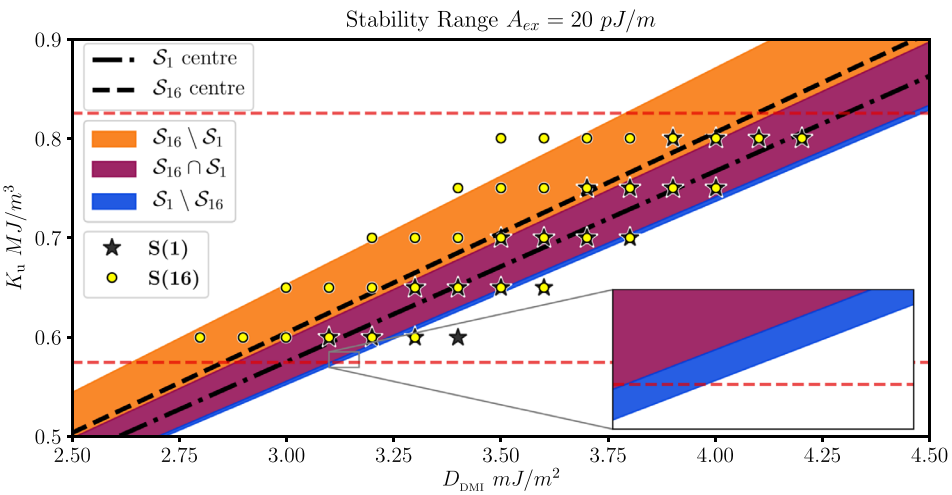

FIG. 2. Stability ranges for $S(1)$ and $S(16)$ bags. Plot for $A_{ex} = 20$ pJ m^{-1}. We define the set $\mathcal{S}_n = \{(D_{DMI}, K_u, A_{ex}) \in \mathbb{R}^3 \mid$ Skyrmion bag oft ype $S(n)$ is stable$\}$; in this plot, we approximate these sets by fixing the exchange constant A_{ex} and shading the areas corresponding to gradients within one σ of the critical gradient taken from Table II. The horizontal dashed lines represent the boundary of the simulations we have performed. The inset highlights that $\mathcal{S}_1 \setminus \mathcal{S}_{16}$ is not empty for this approximation.

TABLE II. Critical line gradients (2 s.f.).

Exchange A_{ex} pJ m^{-1}	Type	Gradient m pm^{-1}	Standard deviation σ pm^{-1}
10	$S(1)$	2.72	0.08
10	$S(16)$	2.84	0.14
15	$S(1)$	2.22	0.08
15	$S(16)$	2.32	0.14
20	$S(1)$	1.92	0.08
20	$S(16)$	2.01	0.16

tested, and therefore, the ideal parameter range to find bags lies within the $|1\sigma|$ range for $S(1)$ (see Fig. 2).

For applications, a stable size of skyrmion bags will be important. We analyze bag diameters as we vary DMI and anisotropy. We find that there are bags, at each set of constants, varying in size by less than 5% from their average width. We analyze the polar angle profiles of the $S(1)$ bags, as shown in Fig. 3, for a range of DMI at $A_{ex} = 20$ pJ m^{-1} and $K_u = 0.7$, by taking the midline, $y = 0$, of the simulated area and extracting the angle at every cell, Fig. 3(b). The outer edge of a bag, in this study, is considered the first cell on the midline, from the left or right hand domain sides, where the polar angle was greater than 150°.

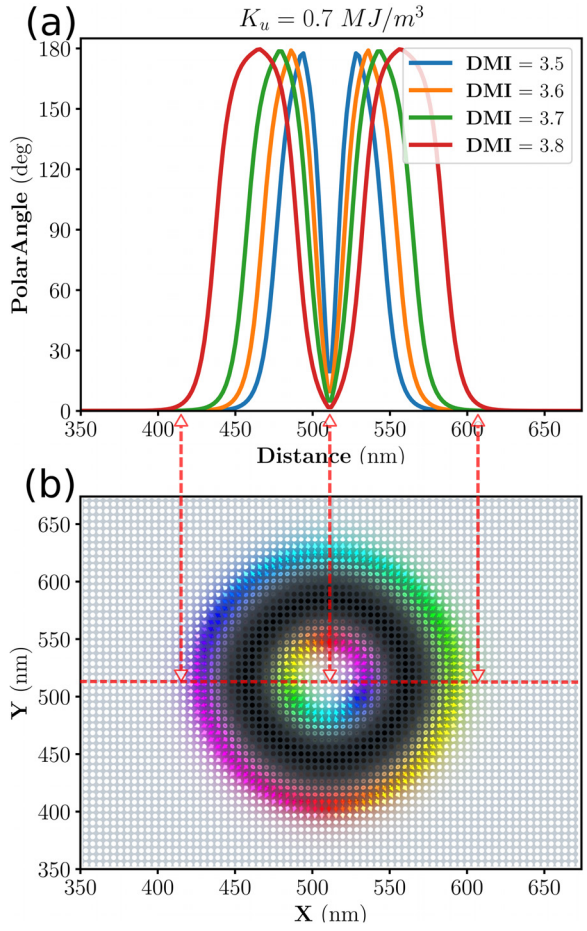

FIG. 3. Polar angle of magnetization profiles of $S(1)$ bags for DMI at $A_{ex} = 20$ pJ m^{-1} and $K_u = 0.7$. (a) Polar profiles. (b) A stable Neèl type skyrmion for $D_{DMI} = 3.8$ mJ m^{-2} and $K_u = 0.7$ MJ m^{-3} with arrowed lines mapping from the centerline of the skyrmion to the appropriate points on the profile (b).

TABLE III. Fitted straight lines at $A_{ex} = 20$ pJ m^{-1} for $S(1)$ (2 s.f.). Fitted values of the anisotropy K_u^{fit} at a given DMI were calculated with Eq. (12) using the value for m in Table II.

Anisotropy K_u MJ m^{-3}	DMI D_{DMI} mJ m^{-2}	Diameter nm	Fitted K_u^{fit} MJ m^{-3}	Difference $\Delta K_u/K_u^{fit}$ %
0.6	3.1	74	0.62	3.5
0.65	3.3	70	0.66	1.75
0.7	3.5	70	0.7	0.2
0.75	3.7	70	0.74	−1.13
0.8	3.9	70	0.78	−2.3

Table III shows that skyrmion bags of similar size can indeed be found as we vary the critical constants of Anisotropy and DMI. We also note that for a fixed exchange energy and anisotropy, increasing DMI within the stable regime increases the bag size super-linearly as can be seen from the profile widths, Fig. 3(a). Hence, for tightness of spin textures, which is important for higher areal density data storage, the lower end of the stable DMI range is to be preferred.

In summary, we have found a range of constants, associated with a linear function and a variation, where we have high confidence that skyrmion bags will be stable. Our analysis shows linear center lines $K_u = m \cdot D_{DMI}$ around which stable $S(1)$ and $S(16)$ bags are found (see Table II). This linear form agrees with the expected form of a Derrick scaling analysis and highlights that corrections from demagnetization act as effective anisotropy.

From the obtained results, we expect that along $S(1)$, skyrmionium, centerline, at any given exchange energy, is the ideal starting point for the seeding and observation of skyrmion bags in thin film multilayers.

Equation (12) should be an effective tool to aid in the experimental realization of skyrmion bags in magnetic multilayers. The existence of suitable experimental methods to vary these parameters should allow fine-tuning of appropriate samples.

Dan Read gratefully acknowledges support from the Leverhulme Trust via an International Academic Fellowship (No. IAF-2018-039). This work was supported in part by the UK Engineering and Physical Sciences Research Council (EPSRC) Grant No. EP/M506473/1. The Titan V GPU used for parts of this research was donated by the NVIDIA Corporation.

REFERENCES

[1]A. Bogdanov and A. Hubert, J. Magn. Magn. Mater. **138**(3), 255–269 (1994).
[2]A. Fert, V. Cros, and J. Sampaio, Nat. Nanotechnol. **8**(3), 152–156 (2013).
[3]A. Fert, N. Reyren, and V. Cros, Nat. Rev. Mater. **2**(7), 17031 (2017).
[4]D. Foster, C. Kind, P. J. Ackerman, J.-S. B. Tai, M. R. Dennis, and I. I. Smalyukh, Nat. Phys. **15**(7), 655–659 (2019).
[5]F. N. Rybakov and N. S. Kiselev, Phys. Rev. B **99**(6), 064437 (2019).

[6]M. Finazzi, M. Savoini, A. R. Khorsand, A. Tsukamoto, A. Itoh, L. Duò, A. Kirilyuk, T. Rasing, and M. Ezawa, Phys. Rev. Lett. **110**(17), 177205 (2013).
[7]X. Zhang, J. Xia, Y. Zhou, D. Wang, X. Liu, W. Zhao, and M. Ezawa, Phys. Rev. B **94**(9), 094420 (2016).
[8]W. Jiang, W. Zhang, G. Yu, M. Benjamin Jungfleisch, P. Upadhyaya, H. Somaily, J. E. Pearson, Y. Tserkovnyak, K. L. Wang, O. Heinonen, S. G. E. te Velthuis, and A. Hoffmann, AIP Adv. **6**(5), 055602 (2016).
[9]F. Hellman, A. Hoffmann, Y. Tserkovnyak, G. S. D. Beach, E. E. Fullerton, C. Leighton, A. H. MacDonald, D. C. Ralph, D. A. Arena, H. A. Dürr *et al.*, Rev. Mod. Phys. **89**(2), 025006 (2017).
[10]H. Yang, O. Boulle, V. Cros, A. Fert, and M. Chshiev, Sci. Rep. **8**(1), 12356 (2018).
[11]A. Cao, X. Zhang, B. Koopmans, S. Peng, Y. Zhang, Z. Wang, S. Yan, H. Yang, and W. Zhao, Nanoscale **10**(25), 12062–12067 (2018).
[12]A. W. J. Wells, P. M. Shepley, C. H. Marrows, and T. A. Moore, Phys. Rev. B **95**(5), 054428 (2017).
[13]J. Hu, P. Wang, J. Zhao, and R. Wu, Adv. Phys.: X **3**(1), 1432415 (2018).
[14]J. Sampaio, V. Cros, S. Rohart, A. Thiaville, and A. Fert, Nat. Nanotechnol. **8**(11), 839–844 (2013).
[15]S. Woo, K. M. Song, H.-S. Han, M.-S. Jung, M.-Y. Im, K.-S. Lee, K. S. Song, P. Fischer, J.-I. Hong, J. W. Choi, B.-C. Min, H. C. Koo, and J. Chang, Nat. Commun. **8**, 15573 (2017).
[16]R. Tomasello, E. Martinez, R. Zivieri, L. Torres, M. Carpentieri, and G. Finocchio, Sci. Rep. **4**, 6784 (2015).
[17]A. Vansteenkiste, J. Leliaert, M. Dvornik, M. Helsen, F. Garcia-Sanchez, and B. Van Waeyenberge, AIP Adv. **4**(10), 107133 (2014).
[18]G. H. Derrick, J. Math. Phys. **5**(9), 1252–1254 (1964).
[19]R. Clausius, London, Edinburgh, Dublin Philosoph. Mag. J. Sci. **40**(265), 122–127 (1870).
[20]R. C. O'Handley, *Modern Magnetic Materials: Principles and Applications* (Wiley, 2000).
[21]A. Bogdanov and A. Hubert, J. Magn. Magn. Mater. **195**(1), 182–192 (1999).
[22]T. W. Anderson and D. A. Darling, Ann. Math. Stat. **23**(2), 193–212 (1952).